Instituto de Engenharia de Sistemas e Computadores de Coimbra

Institute of Systems Engineering and Computers

INESC - Coimbra

Jacinto Estima, Ismael Jesus, Cidália Costa
Fonte, Alberto Cardoso

Geolocation of static events using smartphone measurements from citizens

No. 1 2023

ISSN: 1645-2631

Instituto de Engenharia de Sistemas e Computadores de Coimbra

INESC - Coimbra

Rua Sílvio Lima, Polo II da UC, DEEC; 3030-790 Coimbra; Portugal

www.inescc.pt

The work was supported by the Fundação para a Ciência e a Tecnologia (FCT) under project PCIF/MPG/0128/2017

Geolocation of static events using smartphone measurements from citizens

Preprint

Jacinto Estima[1*], Ismael Jesus[1,2], Cidália Costa Fonte[2], Alberto Cardoso[1]

1. *University of Coimbra, CISUC, Department of Informatics Engineering, Rua Sílvio Lima 030-290 Coimbra, Portugal*
2. *University of Coimbra, INESC Coimbra, Department of Mathematics, Largo D. Dinis, 3000 – 143 Coimbra, Portugal*

* Corresponding author

Abstract

The increasing use of smartphones has led to a surge in crowdsourcing initiatives where citizens collect and upload information. As citizens are more familiar with using their smartphones in various daily life activities, it becomes easier to obtain their participation. Additionally, recent smartphones are equipped with a greater number of sensors, allowing for the collection of measurements that were impossible to obtain with older models. In this paper, we present a novel method for determining the geolocation of static events using citizen contributions. Our method aims to mitigate the errors associated with measured bearings by triangulating all available contributions. This triangulation results in an approximate region that either contains the target location or is very close to it. We tested our method in three experiments, each with a known target location, to assess its reliability. The results were promising, indicating that our approach is particularly useful in applications where high degrees of certainty are not required, such as forest fire ignitions. Combining this method with citizen contributions can provide valuable support to authorities, enabling them to act quickly and effectively in such emergency situations.

Keywords

Volunteered Geographic Information; Orientation; Crowdsourcing; geolocation of static events; Citizen participation

1. Introduction

The use of smartphones by citizens has been massified in the last decades. As citizens are more familiar with using their smartphones in various daily life activities, it becomes easier to obtain their participation in crowdsourcing initiatives through mobile devices, particularly when the relevance of those activities for society is well perceived. Moreover, modern smartphones are nowadays equipped with a variety of sensors, particularly for positioning (e.g., Global Navigation Satellite System (GNSS) receivers) and orientation (e.g., digital compasses) allowing to collect data that otherwise would not be possible. However, the quality of positioning and orientation measurements is key for many applications. Although the accuracy and precision of these sensors have been increasing over time, there are several aspects affecting the quality of their measurements, such as signal blocking or reflections and the multipath effect (Hölzl et al., 2013; Hoseinitabatabaei et al., 2015; Zhang et al., 2018) for GNSS positioning, and calibration errors or the influence of magnetic fields for compass measurements (Odenwald, 2019), to name just a few.

Most studies have been looking at GNSS-based positioning errors and less attention has been paid to compass-based orientation errors, which are key for applications requiring such measurements. They may suffer from external effects, such as magnetic fields in the surroundings (e.g., ferromagnetic materials like cars, power transmission lines, and other metallic objects) and sensor-related noise, mostly associated with the quality of the sensor and its location within the internal layout of the device. Consequently, different smartphone models from different manufacturers have diverse levels of quality (e.g., different levels of quality are applied to devices targeting different segments of buyers), all influencing the accuracy and precision of measurements differently.

Experiments in the field of geology made by Odenwald (2019), comparing a smartphone and a tablet, showed consistent results regarding the first, with azimuth absolute errors around 2 degrees, in contrast to the 20 degrees obtained with the latter. Novakova & Pavlis (2017) developed a case study to assess the precision of two mobile devices for the measurement of planar orientations. Using a smartphone and a tablet, they revealed that the quality of the measurements can be very different among different devices. While the smartphone showed stability and lower errors, the tablet revealed a very unstable quality. Their study suggests that the problems are mainly related to the hardware (i.e., the sensors themselves) and, worse than that, they may be unpredictable. Fonte et al. (2022) performed several experiments to understand the variability of the bearing in different locations with 5 different smartphone models from different manufacturers. The results showed a relatively small standard deviation, with 75% of the values below 1 degree, but a relatively high difference regarding the real bearing measure, in some cases surpassing 20 degrees. Moreover, errors might be systematic or drift through time (e.g., see (Novakova & Pavlis, 2017), (Whitmeyer et al., 2019)).

For applications requiring the contribution of multimedia data (e.g., photos, videos) taken from a distance, the impact of orientation errors can be very relevant given that they are a function of distance. The magnitude of the displacement error can be estimated using Equation 1, where L_i represents the displacement error, perpendicular to the line of sight, $D_i$the distance to the observed location, and δ the orientation error that can assume a right or left direction. For a better understanding of the impact of the distance over the error, Figure 1 provides a visual illustration and Table 1 shows some examples of the error for different distances.

$$L_i = D_i \ sin \ \delta \tag{1}$$

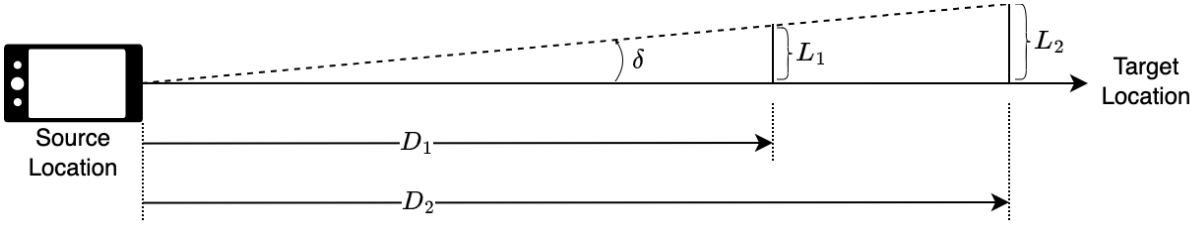

Figure 1 - Orientation inaccuracy δ and its potential impact L_i on the event localization, depending on its distance D_i from the observation site (adapted from (Fonte, Patriarca, et al., 2022))

Table 1 - Displacement error L_i (meters) as a function of the distance D_i between the source location and the target location, and the orientation error (δ).

Orientation error (δ) (degrees)	**Distance D_i(meters)**		
	500	**1000**	**5000**
1	17	35	175
2	35	70	349
5	87	174	872
10	174	347	1736
20	342	684	3420

Given the impact of orientation errors described above, it is of utmost relevance to developing methods that help mitigate the effect of those errors, especially in cases where accuracy is key. Previous studies have looked at this particular issue. Hoseinitabatabaei et al. (2015) proposed a system that uses internal mobile sensors (i.e., accelerometer, magnetic field, among others) to automatically detect and estimate the facing direction of users while they are walking. Their approach works in two phases: (i) first the position of the mobile phone is estimated and, (ii) accordingly, the best algorithm to estimate the direction, from a list of sorted direction algorithms for each position, is used. Kunze et al. (2009) presented a method to estimate the orientation of mobile devices while they were carried out in their user's pockets.

This work proposes an approach to identify the probable geolocation of observed events by combining contributions from multiple volunteers located around a target event. The approach enables: (i) the estimation of errors associated with measured orientations, and (ii) the use of these errors to estimate target regions with several degrees of confidence that are likely to include the observed event. One potentially relevant use case is the detection of

forest fire ignitions. The results show that, even though it was not possible to eliminate the effects of the observed errors, the regions obtained for likely geolocation of the observed events enable the identification of the target's geolocation with several degrees of confidence.

The results demonstrate that, while it wasn't possible to eliminate the effects of observed errors, the identified regions either include the observed event or are very close to it.

The remainder of this paper is organized as follows. Section 2 describes the methodology proposed in this study along with partial results of one experiment to facilitate the understanding; section 3 presents and discusses the results of three experiments (including the one used to provide partial results during the methodology description); section 4 concludes the paper and draws potential directions to follow in future work.

2. Methodology

This section outlines the methodology proposed in this study, which, to the best of our knowledge, has not been tried before. In an ideal scenario, determining the location of a target event (e.g., the event location) from a source location (e.g., the user's location) requires knowledge of the source location coordinates, the direction to the target, and the distance to it. These measures can be taken with the help of a mobile device. However, mobile devices cannot directly measure the distance to a target, and human estimations are often inaccurate. As a result, to rely only on measurements captured by mobile devices, it is necessary to develop strategies that enable the geolocation of the observed event and that enhance accuracy and reduce uncertainty.

The methodology proposed in this paper is divided into two parts. The first part focuses on estimating the orientation errors, processing the uncertainty, and combining the different contributions. In this part, we employed a combination of techniques to estimate the orientation errors and process the uncertainty in the data. We then used a triangulation approach to combine the different contributions and generate an initial region/ set of regions. The second part of the methodology is designed to refine these resulting regions. To do this, we collected measurement data following the first part of this methodology and applied the convex hull concept. We employed an iterative process to adjust the resulting region.

To collect the aforementioned measurements, we used a developed mobile application that collects the user's geolocation obtained via the GNSS receiver, the magnetic bearing pointing towards the target location and the magnetic bearing towards the user's own shadow, which is used to estimate the orientation error. We selected point of interest that was visible from almost anywhere around the city of Coimbra, namely the main tower at the University of Coimbra, as the target location. To simulate people using the mobile app to report an event occurring at this target location, we collected data from various source locations in the field.

2.1. Base geolocation approach

Our methodology triangulates the orientation measurements (i.e., the bearings) from multiple users to estimate the location of static events. The intersection of the bearings gives us an approximation of the area where the event is taking place. This approach requires a minimum of two contributions. If more contributions are available, they are all used to minimize the uncertainty of the location which results in a more accurate location estimate. Figure 2 illustrates this approach using the contributions of four users, where $B_i(i = 1,4)$ represents the magnetic bearings measured by mobile devices. These bearings are measured clockwise and vary between 0° and 360°. The resulting geometry shows the most probable location of the event.

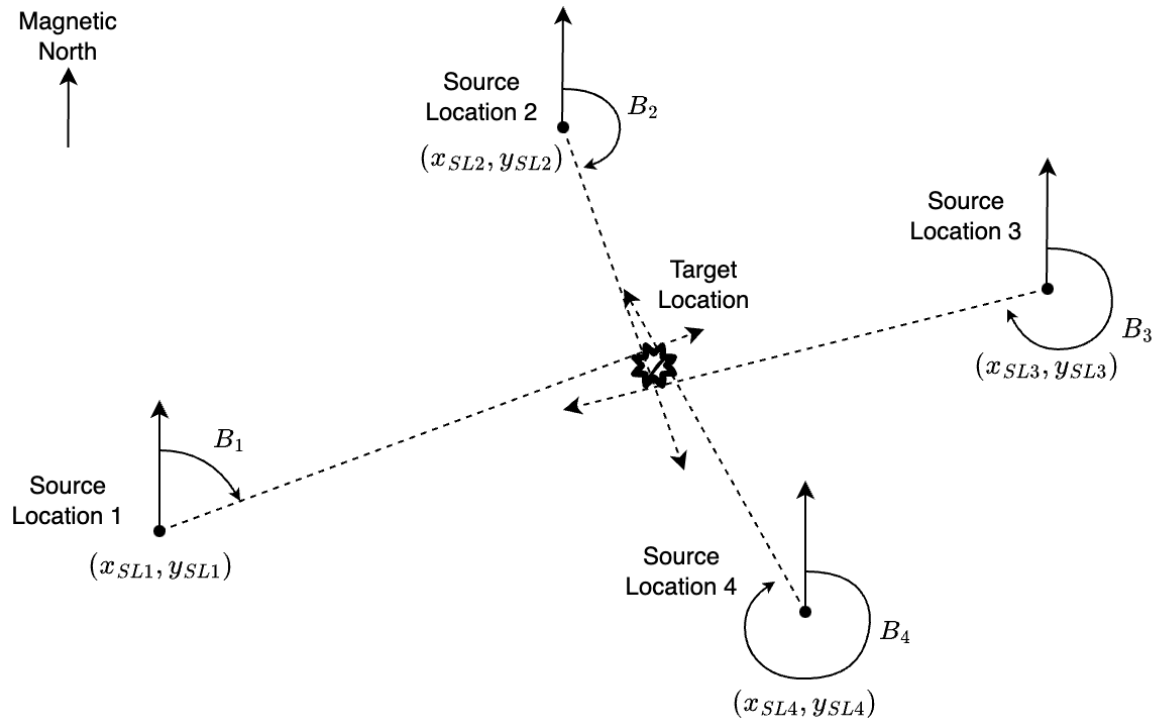

Figure 2 - Event geolocation principle with the contributions of 4 volunteers (adapted from (Fonte, Jesus, et al., 2022))

However, these measurements are often subject to errors. When orientation errors are relatively large, the intersection of lines of sight results in locations far from the true geolocation of the event. To produce an accurate final solution, it's essential to measure and account for such errors.

2.2. Estimating the orientation errors

To minimize the effects of errors in bearing measurements, we propose using the bearing measured towards the shadow of the volunteer. The azimuth of the shadow can be computed from the known azimuth of the sun using the solar position algorithm (Reda & Andreas, 2008), which takes into account the geographic coordinates of the volunteer and the date and time of the measurement. This orientation can then be converted into a magnetic bearing

considering the magnetic declination, which is computed by magnetic observatories. By comparing the computed magnetic bearing with the one measured by the volunteer's smartphone, we can calculate the observation error and use it to correct the bearing measured towards the target location (i.e., the event), hopefully obtaining a more accurate estimate of the true bearing.

Considering that AZ_{sun} is the azimuth of the sun, δ the magnetic declination computed by official magnetic observatories[1] and regularly updated, B_{MS} the measured magnetic bearing of the shadow, and B_{M_TL} the measured magnetic bearing towards the target location. Equations (3), (4) and (5) enable the computation of, respectively: the real magnetic bearing of the shadow (B_{RS}), the magnetic bearing error (ε), and the corrected magnetic bearing towards the target location (B_{C_TL})

$$B_{RS} = AZ_{sun} \pm \delta \pm 180deg, \tag{3}$$

$$\varepsilon = B_{RS} - B_{MS}, \tag{4}$$

$$B_{C\_TL} = B_{M\_TL} + \varepsilon. \tag{5}$$

This procedure is illustrated in Figure 3.

[1] https://intermagnet.github.io/

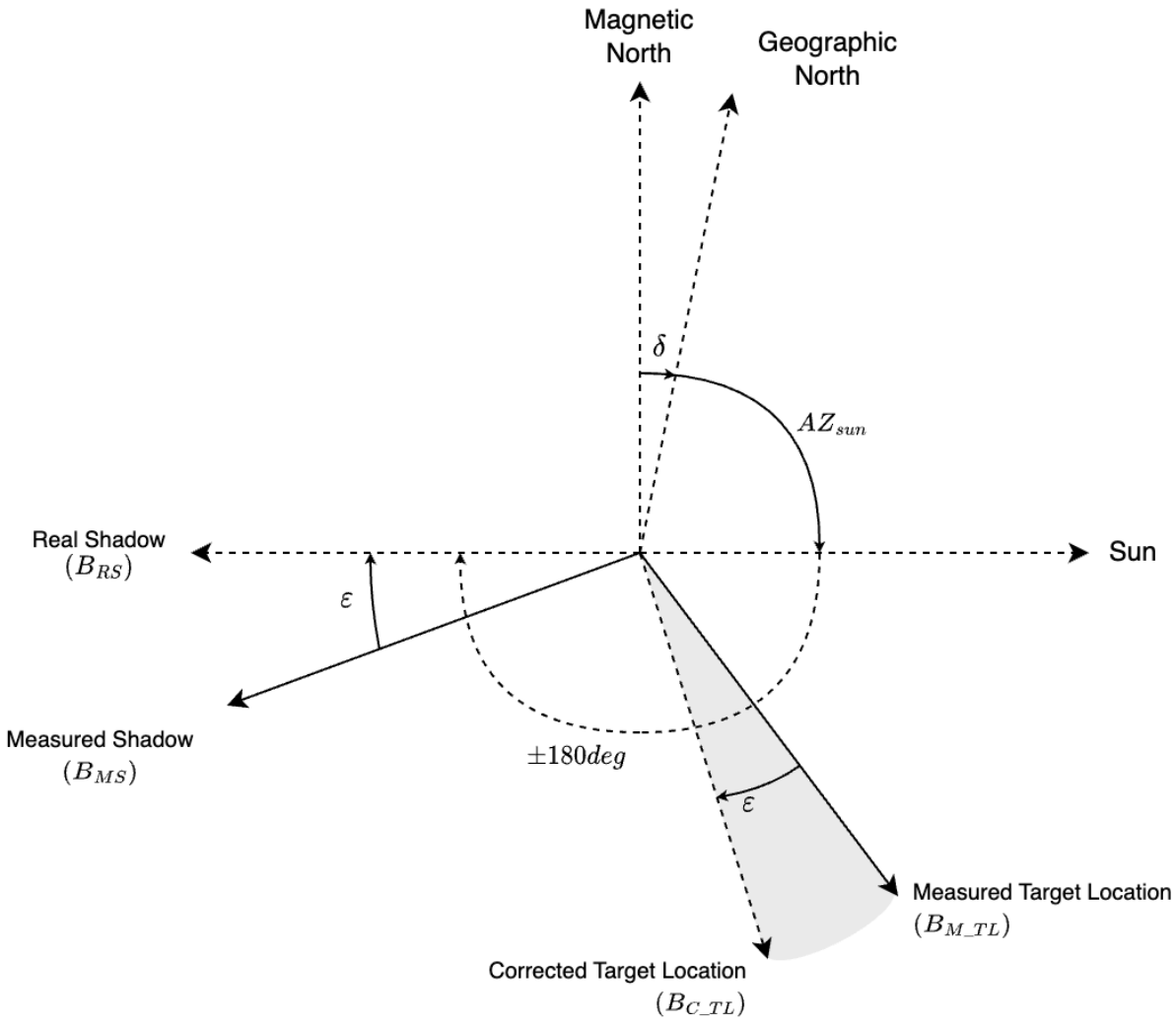

Figure 3 - Relation between the measured and real bearings (adapted from (Fonte, Jesus, et al., 2022))

Fig 4 shows the bearings initially measured towards the target location (left) and their corrected version using the error calculated towards their shadow (right).

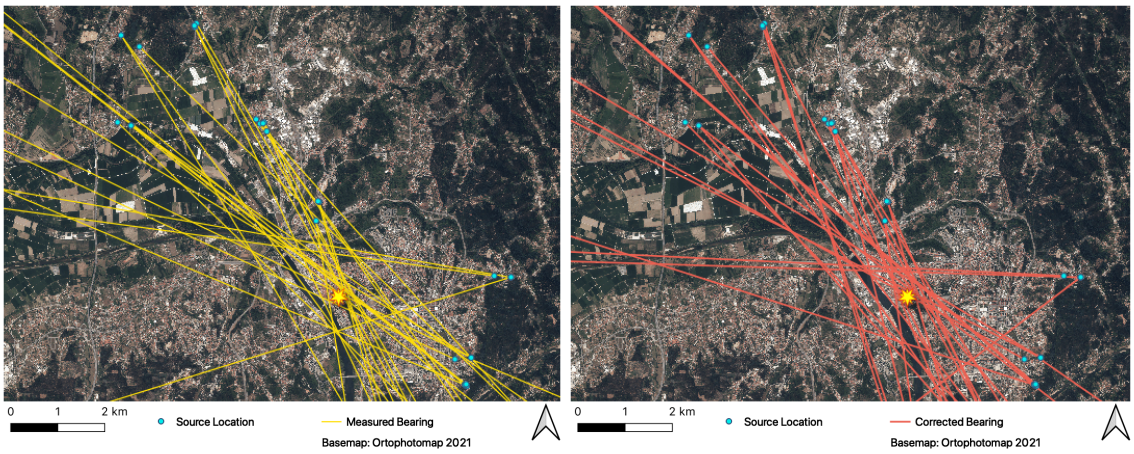

Figure 4 - Initially measured bearings (left) and their corrected version (right)

2.3. Processing the orientation uncertainty

The description of the method provided until now enables the estimation of the orientation error associated with the bearing's measurement. However, as many factors may affect the accuracy of the measured magnetic bearing, which may even change during the time spent to complete a contribution, we added additional conditions to filter and process these data to compute the estimated geolocation of the target location. As in some cases the error in the measured and computed magnetic bearing towards the shadow may be very large, we consider errors larger than 20 degrees to be too significant, and they may indicate that the measurement has been affected by some unknown factors (e.g. magnetic fields in the vicinity or lack of calibration of the compass). Therefore, such errors are considered outliers and the observations are removed from the data processing.

To account for the inherent uncertainty in bearing measurements, we developed a fuzzy approach to capture the variability related to the likelihood of the target location. Rather than representing the bearing towards the target location as a line, we define a funnel-shaped region with its apex at the observer's location and the opening angle equal to the previously calculated error, ε. The bisector of the funnel is the corrected bearing towards the target location, which is obtained by adding the estimated error ε to the measured bearing. Even though this approach accommodates the inherent variability and lack of systematic nature in the errors associated with bearing measurements, tests showed that in most cases it corresponds to a better estimate of the orientation towards the target location than the original measurement, but exceptions may still occur.

The uncertainty inside each funnel-shaped region is expressed with a fuzzy trapezoid centred at the corrected bearings towards the target location, B_{C_TL}. Figure 4 shows a section of the funnel region perpendicular to the line corresponding to the corrected bearing. The core of the fuzzy function (degree of membership equal to 1) has an amplitude of ε, and is centred on the B_{C_TL}. with a width of $\pm {}^{\varepsilon}/_{2}$ for both sides. The support of the fuzzy set has an amplitude of ε for both sides of B_{C_TL} (a total of 2ε), with the degree of membership following a linear interpolation between 1 and 0 (see Figure 4).

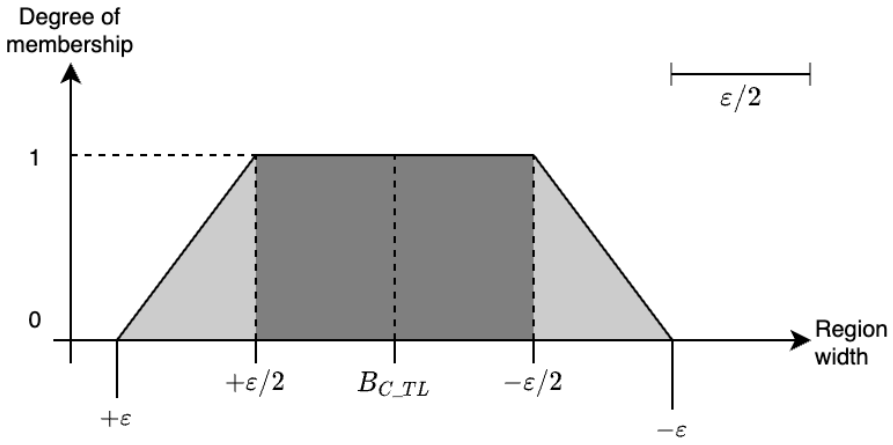

Figure 5 - Trapezoidal fuzzy intervals perpendicular to the bearing to the target location, expressing the orientation uncertainty (extracted from (Fonte, Jesus, et al., 2022))

In practical terms, the funnel is calculated using the raster format and considering the degree of membership assigned to each pixel.

2.4. Integrating contributions

To determine the geolocation of the observed event using the fuzzy sets associated with each contribution, we summed up the raster layers of each contribution, resulting in a final raster layer. The pixel values in this layer ranged from zero (if none of the pixels from the different funnels had a value greater than zero) to the total number of contributions (if all the pixels from the different funnels had a value of one). We can represent the resulting area using different threshold values. For example, we can have a more restricted area using only the maximum value of the raster, which represents 100%, or a broader area using a lower percentage value.

In some cases, the magnitude of the bearing error for certain contributions may be very low (e.g., less than 1 degree). While this might initially seem positive, it could result in a funnel that is more like a line of sight and would not take full advantage of the fuzzy approach described in the previous section. Additionally, since the orientation error is random in nature, these cases could have a negative impact on the integration result of the different contributions. To address this issue, we tested various minimum values for the amplitude of the funnel, ranging from 1 degree to 5 degrees for each side.

Figure 5 shows the integration of 26 contributions towards a target location with varying minimum magnitude values for the funnels. The different shades of red represent different threshold levels (above 0.5 in this case), whereas the darker shades indicate a higher level of belonging to the target location. While lower values of magnitude may provide more accurate results, the figure shows that increasing the minimum magnitude value leads to a more homogenous area at the expense of a slight increase in uncertainty. Based on these findings, we decided to use a minimum magnitude value of 5 degrees for all our experiments.

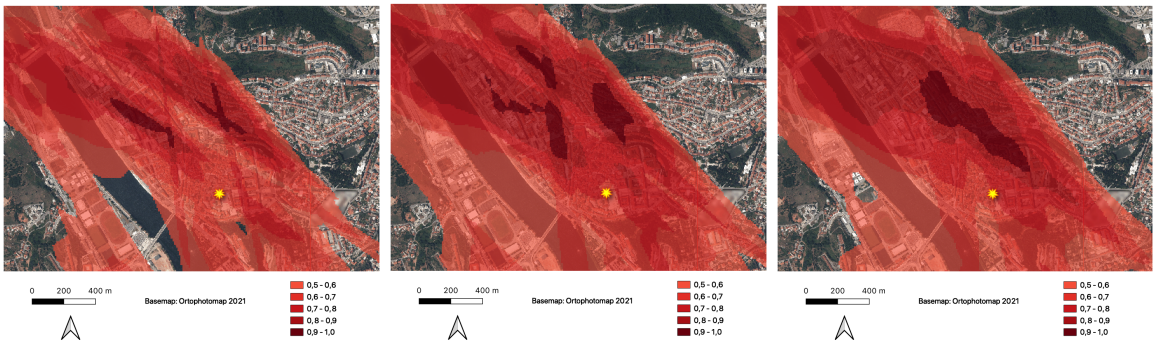

Figure 6 - Integration of x contributions towards a target event (represented as a yellow star). The funnel magnitudes used are, from left to right, 1, 3, and 5 degrees.

2.5. Refining the resulting region(s)

At this point we have a resulting region characterized by a big search space, as we can observe in Figure 5. In this last part of the methodology, we propose an approach to reduce the search space based on the Convex Hull geometry. A Convex Hull is a geometric shape formed by connecting the outermost points of a scatter plot, resulting in a convex polygon that tightly encloses the original data points (De Berg et al., 2008). To perform this calculation, the raster resulting from the integration of several contributions was converted to vector format, resulting in a polygon for each region with pixel values within the predefined threshold classes above 0.5, defined by the following intervals:]0.7, 0.8],]0.8, 0.9], and]0.9, 1.0]).

Starting with the polygons that represent the highest threshold class (i.e.,]0.9, 1.0]), we calculate the Convex Hull geometry that encloses them. Then, we move to the next threshold class in descending order (i.e.,]0.8, 0.9]), and identify the polygons that are within a 500-meter distance from those in the highest threshold class. We then calculate the Convex Hull geometry of the previous Convex Hull with these identified polygons. We repeat this process for the additional threshold classes above 0.5 (i.e.,]0.7, 0.8],]0.6, 0.7], and]0.5, 0.6]), thus covering areas with pixel values above 50% of belonging. It should be noted that the 500-meter distance used to identify new polygons is always measured from the highest threshold class (i.e., from the class]0.9, 1.0].

2.6. Reliability assessment

To assess the reliability of the resulting region, we propose three metrics. First, the area of the largest region, represented by the final Convex Hull geometry obtained after the iteration process, provides an indication of the degree of uncertainty, with larger areas indicating higher uncertainty. Second, the variability of the area among the different levels of belonging (i.e., the different Convex Hull geometries) provides insights into the rate of areal change. Third, we can use the compactness of the geometry's shape, calculated by dividing its area by its perimeter, to understand its complexity. This metric helps us determine whether the shape is more concentrated or elongated. The combination of area and compactness metrics

provides a better understanding of the shape and size of the region, allowing us to assess the degree of uncertainty associated with it.

3. Results and discussion

In this section, we present the results of the experiment described in the Methodology section, where a fictional event was occurring at the main tower of the University of Coimbra. We also include the results of two additional experiments conducted at different target locations, specifically the bridge “Rainha Santa Isabel” and the shopping mall “Fórum Coimbra”, both near Coimbra, for convenience. For each of the three experiments, we show the final Convex Hull geometries for each threshold class above 0.5 (Section 2.5) and their respective metrics as defined in Section 2.6, specifically the area, perimeter, and shape compactness. In these three experiments, the target location is known, and we also provide the shortest distance from each of them to each of the Convex Hull boundaries to help the discussion. We also show the evolution of these metrics throughout the different threshold classes using a set of plots to facilitate the analysis. It is worth noting that the data was collected from several mobile devices of different brands and models to diversify the simulated contributions and approximate them to a real-case experiment.

3.1. Experiment A - University of Coimbra main tower

In this experiment, we collected 31 contributions, but 5 of them had an error higher than 20 degrees and were rejected. Therefore, we used a total of 26 contributions to apply the methodology. Figure 7 displays the Convex Hull geometries obtained from the analysis of the University of Coimbra target location. As we move to lower threshold classes, both the area and perimeter increase and the geometries become more elongated. This trend is reflected in the metric values presented in Table 2. Additionally, the compactness of the geometries decreases, indicating a higher degree of complexity.

Figure 7 - Convex Hull geometries resulting from the analysis of the University of Coimbra main tower

Naturally, the shortest distance from the target location to the Convex Hull geometries decreases as the area increase, reaching zero when the target location falls inside the respective geometry. In this case, the target location is already contained within the]0.7, 0.8] threshold class.

Table 2 - Metrics resulting from the analysis of the University of Coimbra main tower

Threshold class	Area (ha)	Perimeter (meters)	Shape compactness	Distance from the target location to the convex hull geometry (meters)
]0.9, 1.0]	17	20	0,74	214
]0.8, 0.9]	85	45	0,73	116
]0.7, 0.8]	160	58	0,77	0
]0.6, 0.7]	1970	311	0,51	0
]0.5, 0.6]	3305	352	0,58	0

The main feature that stands out in Figure 8 is the inflection point at the threshold class]0.7, 0.8]. Considering the distance between the target location and the Convex Hull geometries, we can see that the target location falls within this class.

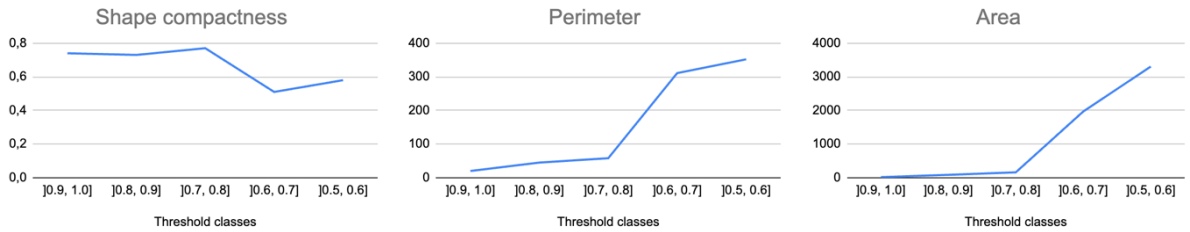

Figure 8 – Plots showing the variation of metrics for the University of Coimbra main tower

3.2. Experiment B - Bridge Rainha Santa Isabel

In this experiment, we collected 19 contributions, but 4 of them had an error higher than 20 degrees and were rejected. Therefore, we used a total of 15 contributions to apply the methodology. Figure 8 shows the Convex Hull geometries obtained from the analysis of the bridge Rainha Santa Isabel target location. Once again, the area and perimeter of the geometries increase and become more elongated as we move to lower threshold classes, which is also reflected in the metric values presented in Table 3. Additionally, the compactness of the geometries mainly decreases, indicating a higher degree of complexity.

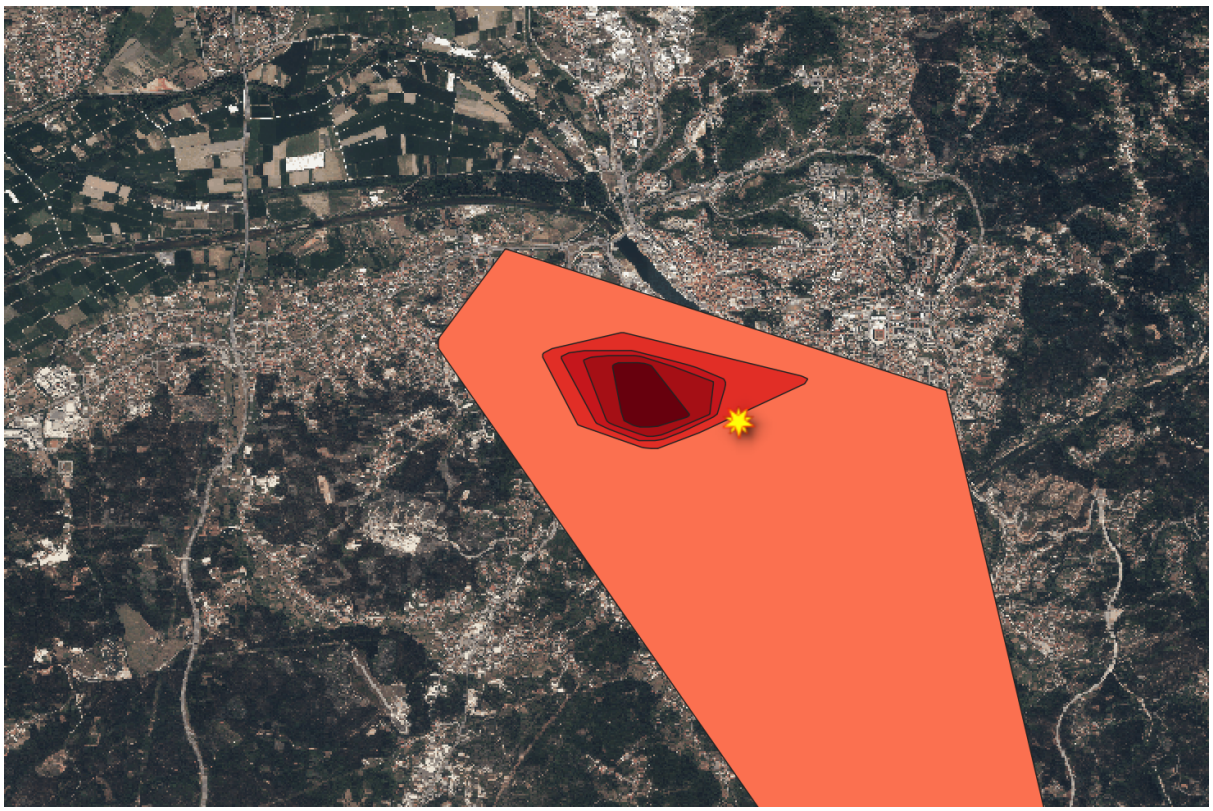

Figure 9 - Convex Hull geometries resulting from the analysis of the bridge "Rainha Santa Isabel".

Likewise, the shortest distance from the target location to the Convex Hull geometries decreases as the area increases, reaching zero when the target location falls inside the

respective geometry. In this case, the target location is contained within the lowest threshold class at]0.5, 0.6].

Table 3 - Metrics resulting from the analysis of the bridge "Rainha Santa Isabel".

Threshold class	Area (ha)	Perimeter (meters)	Shape compactness	Distance from the target location to the convex hull geometry (meters)
]0.9, 1.0]	50	28	0,9	536
]0.8, 0.9]	112	41	0,93	327
]0.7, 0.8]	156	48	0,92	253
]0.6, 0.7]	274	69	0,85	87
]0.5, 0.6]	4093	327	0,69	0

Figure 10 also shows an inflection point at the threshold class]0.6, 0.7] but only for the perimeter and area. The shape compactness decreases smoothly with no inflexion point standing out. Considering the distance between the target location and the Convex Hull geometries, we can see that the target location falls within that class.

Figure 10 – Plots showing the variation of metrics for the bridge "Rainha Santa Isabel".

3.3. Experiment C - Shopping mall Fórum Coimbra

In this experiment, we collected 26 contributions, but 2 of them had an error higher than 20 degrees and were rejected. Therefore, we used a total of 24 contributions to apply the methodology. Figure 11 shows the Convex Hull geometries obtained from the analysis of the shopping mall Fórum Coimbra target location. Once again, the area and perimeter of the geometries increase and become more elongated as we move to lower threshold classes, which is also reflected in the metric values presented in Table 4. In this case, the compactness of the geometries shows a slight increase, indicating a diminishing degree of complexity.

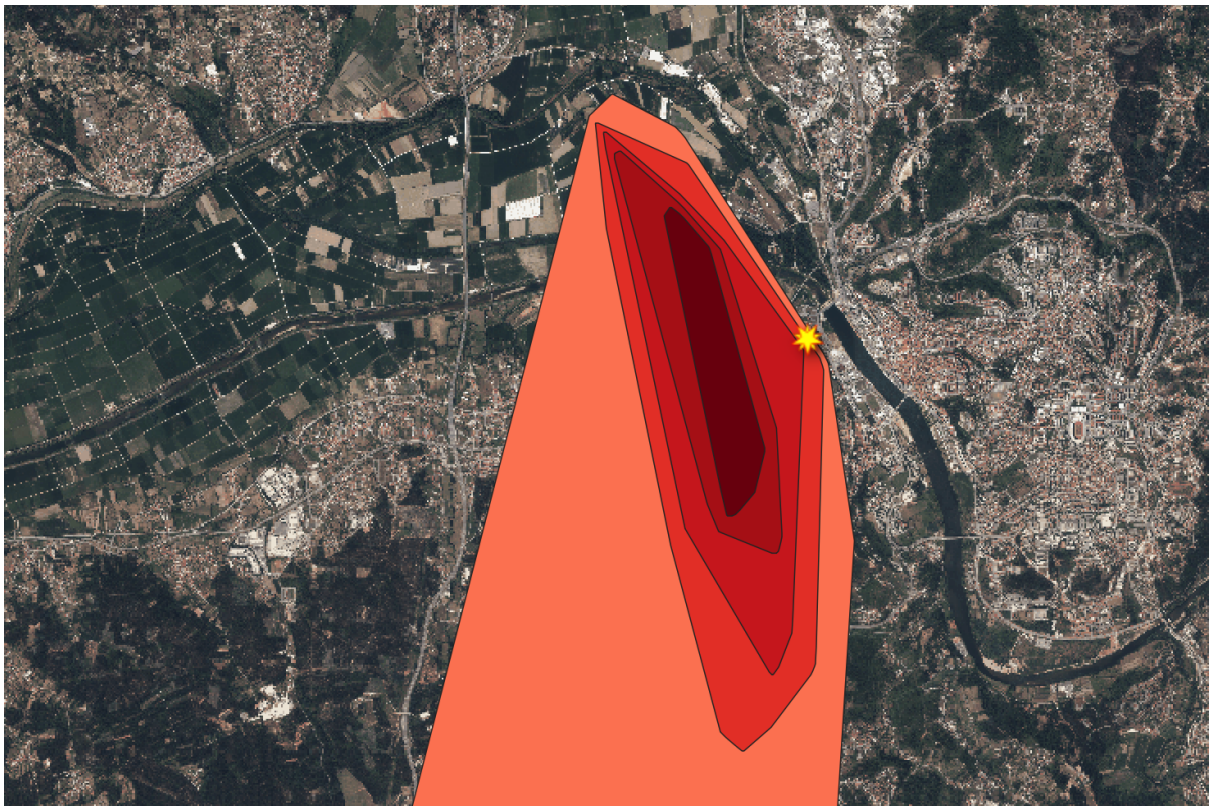

Figure 11 - Convex Hull geometries resulting from the analysis of the shopping mall "Fórum Coimbra".

Besides, the shortest distance from the target location to the Convex Hull geometries decreases as the area increases, reaching zero when the target location falls inside the respective geometry. In this case, the target location is contained within the lowest threshold class at]0.5, 0.6], but the distance to the next class, i.e.,]0.6, 0.7] is very close to zero.

Table 4 - Metrics resulting from the analysis of the shopping mall "Fórum Coimbra".

Threshold class	Area (ha)	Perimeter (meters)	Shape compactness	Distance from the target location to the convex hull geometry (meters)
]0.9, 1.0]	153	73	0,6	786
]0.8, 0.9]	351	101	0,66	632
]0.7, 0.8]	646	133	0,68	110
]0.6, 0.7]	1003	155	0,72	6
]0.5, 0.6]	5783	379	0,71	0

In this experiment, we can also see an inflexion point at the threshold class]0.6, 0.7] only for the perimeter and area, as depicted in Figure 12. The shape compactness increases smoothly with no inflexion point emerging. Considering the distance between the target location and the Convex Hull geometries, we can see that the target location falls within that class.

Figure 12 – Plots showing the variation of metrics for the shopping mall "Fórum Coimbra".

3.4. Discussion

In a real-world scenario, the geolocation of the target is usually unknown. However, to evaluate the effectiveness of this methodology, we conducted the three experiments described in this section, with known target locations. This allowed us to compare the results with the actual geolocation of the targets. Based on the analysis of these experiments, it appears that the inflexion point can be a useful indicator for selecting the smallest geometry that can include the potential target location or have it at a negligible distance (depending on the application). In experiment A, the inflexion point occurs at the threshold]0.7, 0.8] and the target location is included in that geometry. In experiment B, the inflexion point appears at the threshold]0.6, 0.7] and the target location is included in the geometry of the lower class, i.e.,]0.5, 0.6]. If we consider the inflexion class, the shortest distance between the target location and the geometry boundary is 87 meters. In experiment C, the scenario is similar to experiment B, except that the shortest distance between the target location and the geometry boundary of the inflexion class decreases to a negligible value of 6 meters.

4. Conclusion

This paper proposes an innovative method to calculate the approximate geolocation of static events using volunteer contributions taken from a distance using smartphones. The approach helps minimize orientation errors usually associated with the measurement of bearings which is one of the most difficult error types to tackle given its random nature. We performed three experiments targeting three different but known locations and compared them with the resulting areas. The results demonstrated that our method is able to determine regions containing the target location with different degrees of belonging, or with a negligible distance to it from their boundaries. Plotting the different reliance metrics throughout the threshold classes showed inflexion points that were good indicators to select the best Convex Hull geometry. In one experiment the target location was contained by that geometry whereas in the other experiments, the target location was at a small distance.

Such a method can be beneficial in various applications which do not require a high degree of certainty, such as forest fire detection. In this case, citizens can use their smartphones to collect and submit the required measurements, helping authorities act quickly.

In reality, forest fires are not static events. This approach can be further extended to support events that move over time. This is an interesting idea for a future research avenue. Although one may think to replicate the approach proposed here at various t times, the problem is much more complex than that. At different time steps, each contribution should have an associated weight that decreases over time. In this way, we expect this method to geolocate the event's beginning and monitor its progression over time and space.

Funding

This work was partially funded by FCT - Foundation for Science and Technology, I.P./MCTES through national funds (PIDDAC), within the scope of CISUC R&D Unit - UIDB/00326/2020 or project code UIDP/00326/2020, the grant number UID/MULTI/00308/2019, and the project Fireloc with grant number PCIF/MPG/0128/2017.

References

De Berg, M., Cheong, O., Van Kreveld, M., & Overmars, M. (2008). *Computational Geometry: Algorithms and Applications*. Springer. https://doi.org/10.1007/978-3-540-77974-2

Fonte, C. C., Jesus, I., Pereira, C., Cardoso, A., Estima, J., Patriarca, J., & Almeida, J.-P. de. (2022). The FireLoc system—Methodologies for geolocating the observed fires. In D. X. Viegas & L. M. Ribeiro, *Advances in Forest Fire Research 2022* (1.ª Edição, pp. 400–404). Imprensa da Universidade de Coimbra. https://doi.org/10.14195/978-989-26-2298-9_64

Fonte, C. C., Patriarca, J., Almeida, J.-P., Cardoso, A., Estima, J., & Silvestre, D. (2022). *Quality assessment of positioning and orientation data collected by mobile devices*. Instituto de Engenharia de Sistemas e Computadores de Coimbra. https://www.uc.pt/en/org/inescc/res_reports_docs/RR_01_2022

Hölzl, M., Neumeier, R., & Ostermayer, G. (2013). Analysis of Compass Sensor Accuracy on Several Mobile Devices in an Industrial Environment. In R. Moreno-Díaz, F. Pichler, & A. Quesada-Arencibia (Eds.), *Computer Aided Systems Theory—EUROCAST 2013* (Vol. 8112, pp. 381–389). Springer Berlin Heidelberg. https://doi.org/10.1007/978-3-642-53862-9_49

Hoseinitabatabaei, S. A., Gluhak, A., & Tafazolli, R. (2015). Towards a position and orientation independent approach for pervasive observation of user direction with mobile phones. *Pervasive and Mobile Computing*, *17*, 23–42. https://doi.org/10.1016/j.pmcj.2014.02.002

Kunze, K., Lukowicz, P., Partridge, K., & Begole, B. (2009). Which Way Am I Facing: Inferring Horizontal Device Orientation from an Accelerometer Signal. *2009 International Symposium on Wearable Computers*, 149–150. https://doi.org/10.1109/ISWC.2009.33

Novakova, L., & Pavlis, T. L. (2017). Assessment of the precision of smart phones and tablets for measurement of planar orientations: A case study. *Journal of Structural Geology*, *97*, 93–

103. https://doi.org/10.1016/j.jsg.2017.02.015

Odenwald, S. (2019). *Guide To Smartphone Sensors*. NASA Space Science Education Consortium. https://spacemath.gsfc.nasa.gov/Sensor/SensorsBook.pdf

Reda, I., & Andreas, A. (2008). *Solar Position Algorithm for Solar Radiation Applications (Revised)* (NREL/TP-560-34302, 15003974; p. NREL/TP-560-34302, 15003974). https://doi.org/10.2172/15003974

Whitmeyer, S. J., Pyle, E. J., Pavlis, T. L., Swanger, W., & Roberts, L. (2019). Modern approaches to field data collection and mapping: Digital methods, crowdsourcing, and the future of statistical analyses. *Journal of Structural Geology*, *125*, 29–40. https://doi.org/10.1016/j.jsg.2018.06.023

Zhang, X., Tao, X., Zhu, F., Shi, X., & Wang, F. (2018). Quality assessment of GNSS observations from an Android N smartphone and positioning performance analysis using time-differenced filtering approach. *GPS Solutions*, *22*(3), 70. https://doi.org/10.1007/s10291-018-0736-8